A multi-century, tree-ring-derived perspective of the North Cascades (USA) 2014–2016 snow drought

Grant L. Harley[1] · R. Stockton Maxwell[2] · Bryan A. Black[3] · Matthew F. Bekker[4]

Abstract

Cool-season precipitation is a critical component of western North American water supplies. In recent decades, snow water equivalent (snowpack) has declined dramatically, culminating in record lows along the northern Cascade Range, USA, during the winters of 2014 and 2015. Given the brevity of observational records, the extent to which these recent trends exceed historical ranges of variability remains poorly understood. Here, we use a network of 30 tree-ring chronologies to reconstruct April 1 snowpack in the northern Cascade Mountains (Washington, USA) over the past ca. 400 years that accounts for 62% of the instrumental period variability. The reconstruction is characterized by considerable interannual- to interdecadal-scale variability. Yet, the most conspicuous feature is a decline that began in the mid-1970s concurrent with a shift to above-average air temperature which is accelerated through to the most recent years of the record. The 2014–2016 snow drought, especially snow conditions during the 2015 winter, across the northern Cascades is unprecedented within the context of the last 400 years. The reconstruction is characterized by considerable interannual- to interdecadal-scale variability, but a conspicuous decline emerged in the mid-1970s and accelerated through to the most recent years of the record to levels below the pre-industrial envelope of variability. This decline culminated in the 2014–2016 northern Cascade Mountains snow drought, which is unprecedented within the context of the last 400 years. Not only is the twentieth–twenty-first century period characterized by the rapid decline in snowpack conditions, it is also highly volatile. Extreme flips in snowpack conditions (year-to-year changes between <5th and >95th percentiles) during the twentieth and twenty-first centuries were anomalous within the context of the record. These patterns described for the North Cascades are concurrent with anomalously low snowpack in the Sierra Nevada Mountains of California, and thus part of a broader

✉ Grant L. Harley
    gharley@uidaho.edu

Extended author information available on the last page of the article.

trend toward reduced snowpack in western North America. This decline will fundamentally impact regional drought and hydrography in North Cascadia and is likely the combined result of rising temperatures, weakening

1 Introduction

Within montane environments of the western United States (US), snowpack influences runoff regimes (Bales et al. 2006; Barnett et al. 2008), stream ecosystem structure and function (Hauer et al. 1997), wildfire frequency and intensity (Westerling et al. 2006; Littell et al. 2009), and water and air temperatures (Flanner et al. 2011; Pederson et al. 2010). Over recent decades, however, snowpack (snow water equivalent, SWE) has declined substantially throughout the western US (Mote 2003; Mote et al. 2005). Snowmelt and glacial runoff along the North Cascades are critical for community water supply in the region (e.g., Seattle, Tacoma, Olympia, Everett), as well as hydropower, agriculture, and protected and endangered native cold-water fish populations.

During the winters of 2014 and 2015, the North Cascades region (US States of Oregon and Washington) experienced record-low snowpack levels within the context of the instrumental period (since ca. 1920–1930s). As a precursor to this event, sea surface temperatures (SSTs) in the northeast Pacific were anomalously warm during the previous-year winter (2013). Warming continued and expanded into the spring of 2014 coincident with anomalously high sea level pressure. This warming pattern combined with warm air temperatures and the amount and timing of winter precipitation culminated in record-low snowpack levels in the winters of 2014 and 2015 (Mote et al. 2005; Cooper et al. 2016). The severity of this event led the State of Washington to declare a drought emergency in May 2015, and forecasts suggest snowpack declines will continue through the twenty-first century with grave implications for western North American water supplies (Mote et al. 2005).

Although recent snowpack declines in the US Pacific Northwest are unprecedented in observational records, these baselines span only the past several decades. Longer histories are needed to (1) more fully characterize snowpack range and variability and (2) provide historical context to extreme events such as the 2014–2015 snow drought. In the western US, moisture variability is the primary limiting factor of annual radial tree growth (Fritts 1976). Tree-ring time series are commonly used to reconstruct precipitation (e.g., Graumlich 1987; Salzer and Kipfmueller 2005; Meko et al. 2007; Stahle et al., 2009; Griffin et al. 2013), drought (Stockton and Meko 1975; Cook et al. 1999, 2004; Woodhouse et al. 2010; Oliver et al. 2019), and streamflow (Stockton and Jacoby 1976; Woodhouse et al. 2006, 2012; Margolis et al. 2011; Bekker et al. 2014; Harley and Maxwell 2018). However, fewer studies have used tree rings to assess historical snowpack variability (Woodhouse 2003; Pederson et al. 2011; Belmecheri et al. 2016; Peterson and Peterson 1994; Perkins and Swetnam 1996; Watson and Luckman 2016), and no reconstructions are available for the Cascade Mountains of the US Pacific Northwest. Here, we use a multi-species network of existing, updated, and new tree-ring chronologies to reconstruct north Cascade Mountain snowpack and thereby evaluate longer-term ranges of variability and provide context for twentieth and twenty-first century trends.

2 Data and methods

2.1 Instrumental snowpack data

We gathered instrumental snow water equivalent (SWE) data (April 1 1938–2018) from 18 Natural Resources Conservation Service (NRCS) SNOW/SNOTEL stations along the North Cascades (Fig. 1). We initially screened the stations based on length and completeness of the record, degree of inter-correlation among stations (e.g., principal component analysis (PCA), correlation matrix), and normality of the data. Out of the total 18 stations initially gathered, 10 were excluded from the network because of non-normality, incomplete/missing data, or dissimilarity with other stations. The remaining 8 stations were well distributed across a broad region of the northern Cascades, ranging in elevation between 742 m (Tunnel Avenue) and 1981 m (Cloudy Pass) and spanning from Mt. Rainier (Cayuse Pass; 46.87 °N) to Harts Pass (48.72 °N) near the Canadian border. These records included data from the SNOW/SNOTEL networks and had a common period of overlap spanning 1938–2018
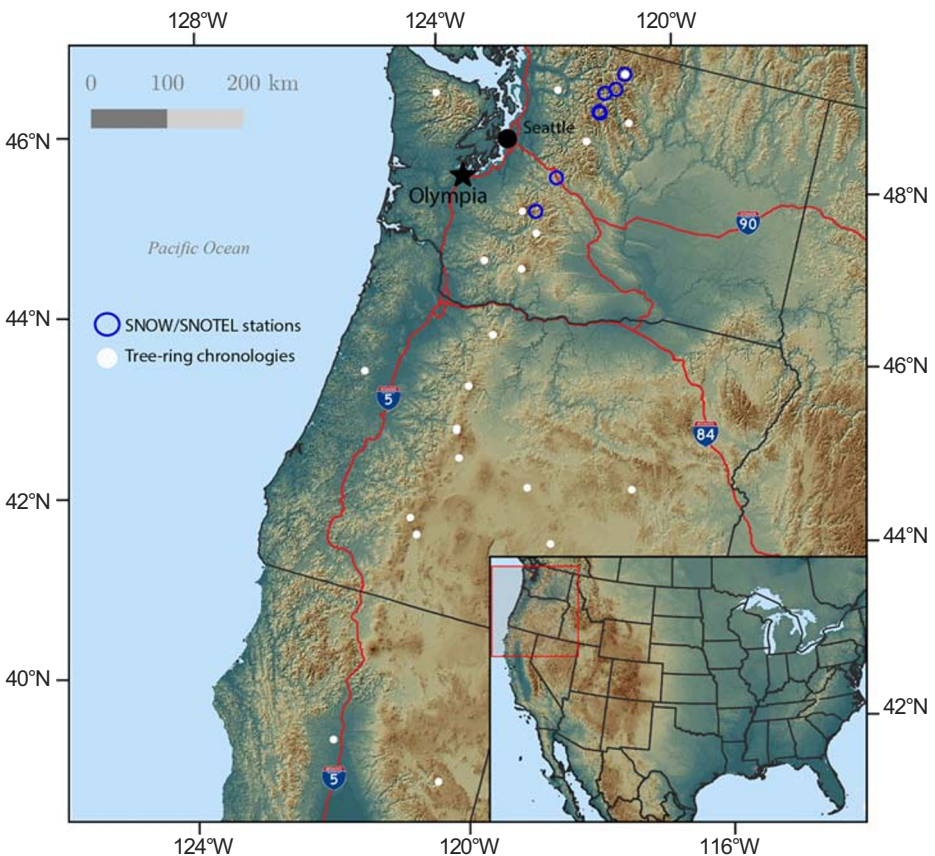

Fig. 1 North Cascades snowpack study area map. Plotted are locations of the 8 SNOW/SNOTEL stations used to compile the instrumental April 1 snow water equivalent (SWE) data during the period 1938–1980 shown with the network of tree-ring chronologies ($n = 30$) used for the reconstruction

Table 1 Information for northern Cascade Mountain Range snow stations used for the April 1 SWE reconstruction

Name	ID	Elevation (m)	°N	°W	Installed (year)
Cloudy Pass	20A22	1981	48.21	−120.92	1927
Little Meadows	20A24	1593	48.20	−120.90	1927
Lyman Lake	20A23	1798	48.20	−120.92	1928
Park Creek Ridge	20A12	1402	48.44	−120.91	1928
Rainy Pass	20A09	1456	48.52	−120.74	1930
Cayuse Pass	21C06	1606	46.87	−121.53	1938
Tunnel Avenue	21B08	742	47.32	−121.34	1938
Harts Pass	20A05S	1978	48.72	−120.66	1938

(Table 1). All 8 stations shared common trends and variance (Fig. S1), strongly and positively correlated (all $p < 0.01$) with each other (Fig. 2), and strongly and positively loaded on PC_1, which accounted for 84% of the variance (Fig. S2). Given the strong agreement among retained SWE stations and the normal distribution of the data (Fig. 2), within each station, we normalized mean April 1 SWE over the common interval and used the mean of these anomalies as the predictand for the reconstruction.
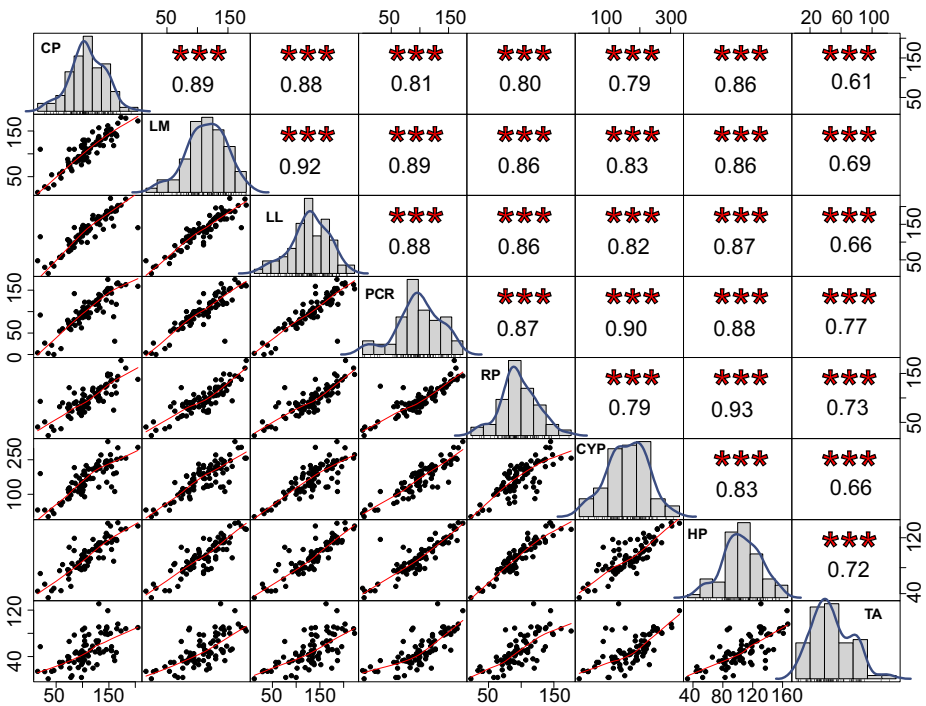

Fig. 2 Snow station agreement. Instrumental correlation matrix (*** denotes $p < 0.01$) between the 8 snow stations included in the April 1 SWE reconstruction plotted with distribution histograms and scatter plots. CP, Cloudy Pass; LM, Little Meadows; LL, Lyman Lake; PCR, Park Creek Ridge; RP, Rainy Pass; CYP, Cayuse Pass; HP, Harts Pass; TA, Tunnel Avenue. Both x- and y-axis limits differ

2.2 Tree-ring network

Tree-ring data for the reconstruction came from (1) existing site collections from the states of Washington and Oregon (US) on the International Tree-Ring Data Bank (ITRDB; https://www.ncdc.noaa.gov), and (2) new site/updated chronologies. To help define a spatial region from which to pull initial chronologies for the candidate pool from the ITRDB, collections were first screened as to whether they were located within the moisture-sensitive footprint of the instrumental snowpack record. A field correlation analysis was conducted between the instrumental snowpack data and the gridded CRU TS3.24 0.5 ° precipitation field during the period 1901–2018 (c.f. Maxwell et al. 2017; Harley et al. 2017; Harley and Maxwell 2018), and chronologies were retained if they fell within the region for which correlations were significant at the $\alpha = 0.01$ level.

After this first screening, 133 ITRDB chronologies were retained representing species common to the Pacific Northwest region (e.g., *Pseudotsuga menziesii* Mirb. Franco; *Tsuga mertensiana* Bong. Carrière; *Larix lyallii* Parl.) over the common period 1830–1980. This pool of candidate chronologies included one new collection (Mary's Peak) and one existing collection (Mt. Rainier High) that we updated (Table S1). At Mary's Peak and Mount Rainier, we extracted two cores from 15–20 trees with an increment borer. Tree cores were prepared and crossdated using methods standard to the field of dendrochronology (Speer 2010). We used the program COFECHA as a crossdating check on new and ITRDB chronologies (Holmes 1983), and any obvious dating errors were cleaned by removing problematic measurement time series or segments therein if near the start or end date. We then used the RCSigFree program to standardize each tree-ring series interactively using signal-free standardization (Melvin and Briffa 2008) in which the base curve was a $\frac{2}{3}$ smoothing spline (i.e., these splines had an amplitude response of 0.50 at periods associated with 67% of each series length (Cook and Peters 1981) and were chosen to retain as much climate signal as possible while removing non-climatic signals related to disturbance and age-related tree-ring growth trends). We chose signal-free standardization to reduce trend distortion whereby medium-frequency variance (i.e., decadal-centennial) leveraged the detrending function near the ends of the record (Melvin and Briffa 2008). To account for the effect of diminishing sample size back through time, we truncated each chronology where the expressed population signal (EPS) statistic fell below a threshold of 0.85 (Wigley et al. 1984). As for the updated chronologies, Mary's Peak is a *P. menziesii* collection that spans the period 1566–2013, and the updated *T. mertensiana* Mt. Rainier High (WA103) chronology now spans 1652–2015.

2.3 Reconstruction model

To reconstruct April 1 SWE for the North Cascades, we chose a nested principal components regression (PCR) model, which accounted for the decrease in the number of predictor chronologies back through time (Cook et al. 1999, 2004, 2007, 2007). In an initial screening phase, tree-ring predictors and snowpack data were pre-whitened to provide a conservative estimate of climate-growth relationships that were not subject to inflation via autocorrelation. Chronologies were retained if they were significantly ($p < 0.01$) related to April 1 SWE over the common period (1938–1980) in the Pearson, Robust Pearson, and Spearman correlation tests. For those tree-ring sites that were significant, their original chronologies (without pre-whitening) were included in the PCR at time t and $t+1$ because of known preconditioning effects of previous-year water availability on current-year tree growth (Fritts 1976). Following the Kaiser-Guttman rule (Guttman 1954; Kaiser 1960), the first n

eigenvectors with eigenvalues >1 were retained for the multiple regression. The final subset of PCs in the regression model was determined by using the minimum Akaike information criterion (AIC), which includes a penalty term for increasing the number of predictors in the model (Akaike 1974).

The common period (1938–1980) was split into two equal periods for calibration (1938–1959) and verification (1960–1980) of the nested PCR models. Calibration models were verified using two rigorous tests of fit, the reduction of error statistic (RE), and coefficient of efficiency (CE) (Fritts 1976; Cook et al. 1999). Given that RE ranges from $-\infty$ to $+1$, a positive RE denotes that the calibration model is more skillful than the mean of the instrumental data during the calibration period. The CE has the same range and calculation, yet it relies on the verification period mean for a baseline of predictive skill and is thus more difficult to pass (value >0). We produced the final reconstruction by calibrating on the full instrumental period (1938–1980). After each nest was calculated, SWE estimates along with each set of calibration and verification statistics were spliced together for the entire reconstruction length.

2.4 Model uncertainty

We assessed model uncertainty using maximum entropy bootstrapping (Vinod et al. 2009); MEBoot) applied to the tree-ring predictors and SWE data with $n = 300$ replicates. MEBoot estimates uncertainty by producing an empirical probability distribution for each year and thus can generate values outside the boundaries of the input data to more effectively simulate the underlying theoretical population (Cook et al. 2013). Other advantages of the MEBoot process are that it does not assume stationarity, it maintains the autocorrelation structure of the time series, and it calculates semiparametric uncertainty estimates for the calibration and verification statistics (see Cook et al. 2013, for details).

2.5 Reconstruction analyses

In addition to calculating standardized anomalies (e.g., z-scores) to assess the long-term trends in SWE, we calculated an index to quantify volatility. We characterized extreme SWE "flips" during consecutive years in the reconstruction by calculating a flip index (i) (c.f. Loecke et al. 2017) as

$$i = \frac{\text{SWE}\,(t+1)\,-\,t}{\text{SWE}\,(t\,+\,(t+1))}$$

for which the SWE value of a given year (t) was subtracted from the value of the following year (t+1), then divided by the total SWE over the 2-year period (t+(t+1)). Positive i values indicated shifts from lower (dry) to higher (wet) SWE conditions, whereas negative values indicated shifts from higher (wet) to lower (dry) snowpack. We defined extreme flips by tallying i values that were <5th percentile (dry) and >95th percentile during the period 1580–2018.

3 Results/discussion

3.1 Tree-ring data

Screening via the moisture-sensitive footprint and then screening for correlation between pre-whitened chronologies and snow data reduced the original candidate pool of 133

chronologies to 30 retained for modeling (Table S1). All retained chronologies correlated negatively with SWE, such that wide (narrow) growth rings were associated with low (high) snowpack years. This negative relationship between tree rings and SWE has been demonstrated previously in the Cascades (Graumlich and Brubaker 1986) and the Canadian Cascades (Hart et al. 2010; Starheim et al. 2013; Coulthard et al. 2016; Watson and Luckman 2016). At the start of the growing season, cambial reactivation and root hydraulic conductance can be delayed by late-melting snow that persists on the landscape, lowering soil temperature (e.g., Hansen-Bristow 1986; Graumlich and Brubaker 1986) and thereby limiting the width of the annual growth ring. The correlation of retained chronologies to SWE ranged from $r = -0.62$ (the updated Mt. Hood High and Mt Hood Medium) to -0.37 (Crater Lake Medium) during the period 1938–1980. Of the 30 chronologies retained for modeling, 29 were downloaded from the ITRDB, with the one new collection of Mary's Peak ($r = -0.39$).

Table 2 Nested reconstruction model statistics. North Cascades April 1 SWE nested reconstruction model statistics, including the common period model (CP) with backward (B) and forward (F) model nests for the period 870–2013 CE

Nest	Period	NTR	EV1	ORD	CR^2	VR^2	VRE	VCE	RMSE
F5	1830–2013	1	1	1	0.10	0.35	0.17	0.11	29.5
F4	1830–2010	2	2	1	0.20	0.38	0.18	0.11	29.5
F3	1830–2005	4	2	2	0.26	0.36	0.35	0.32	25.2
F2	1830–1990	19	4	2	0.43	0.33	0.34	0.32	22.7
F1	1830–1985	23	5	2	0.59	0.58	0.58	0.58	19.5
CP	1830–1980	30	5	2	0.62	0.71	0.71	0.72	19.1
B2	1820–1829	29	5	2	0.62	0.66	0.65	0.65	19.2
B3	1810–1819	28	5	2	0.62	0.67	0.66	0.67	19.2
B4	1790–1809	27	5	2	0.61	0.60	0.59	0.60	19.5
B5	1780–1789	24	4	2	0.57	0.51	0.50	0.51	20.7
B6	1770–1779	22	4	2	0.56	0.54	0.53	0.53	20.9
B7	1760–1769	21	4	2	0.57	0.53	0.52	0.53	20.8
B8	1740–1759	20	4	2	0.55	0.53	0.52	0.53	21.0
B9	1730–1729	18	4	2	0.57	0.53	0.52	0.52	20.9
B10	1710–1729	17	4	2	0.57	0.54	0.53	0.54	20.8
B11	1680–1709	16	4	2	0.57	0.56	0.55	0.55	20.8
B12	1670–1679	13	3	1	0.57	0.56	0.52	0.52	20.5
B13	1630–1769	12	3	1	0.58	0.54	0.53	0.53	20.5
B14	1610–1629	11	3	1	0.58	0.60	0.59	0.58	20.4
B15	1590–1609	9	3	1	0.55	0.57	0.55	0.56	20.7
B16	1580–1589	6	2	1	0.43	0.34	0.33	0.32	23.4
B17	1550–1569	4	2	1	0.40	0.30	0.29	0.27	24.0
B18	1440–1549	3	1	1	0.21	0.16	0.16	0.13	27.3
B19	870–1439	1	1	1	0.15	0.05	0.007	0.006	28.3

NTR, number of tree-ring chronologies; *EV1*, number of eigenvectors with eigenvalues >1.0; *ORD*, eigenvalue order cutoff determined from AIC; CR^2/VR^2, calibration/verification period coefficient of determination; *VRE/VCE*, verification period reduction of error/coefficient of efficiency; *RMSE*, root mean-squared error

3.2 Model calibration and verification

The common period model spanned the period 1830–1980 and included 2 PCs (PC$_1$ and PC$_2$) that explained 62% of the instrumental SWE variance from 1938–1980 (Table 2). Including the common period, the reconstruction comprised 19 backward nests extending to the year 870. We also performed forward nests from 1981 to 2013 to demonstrate that trees track the instrumental record over the snow drought and highlight the need for updated chronologies in the region. Going backwards in time, the model nests remained robust, explaining over 40% of the instrumental variance with strong and positive RE and CE values until 1580. The reconstruction remained valid back to 870, however, as the number of tree-ring chronologies (NTR) was reduced to <6 at 1580, the CR^2 and VR^2 dropped and the models weakened. Although the 870–1439 nest passed validation tests (positive RE and CE), the model was weak, explaining only 15% of the instrumental variance. Given that the overarching objective of this paper was to compare the modern snow drought with a record that extended beyond the instrumental period, we truncated the reconstruction at 1580, as this was the last backward nest that explains >40% of the instrumental variance.

As expected, the forward model nests dropped rapidly with NTR and in conjunction with all validation statistics (e.g., CR^2, VR^2, RE, CE, RMSE), though models were robust until ca. 1990, after which the NTR dropped from 19 to 4. Yet even with low sample depth,
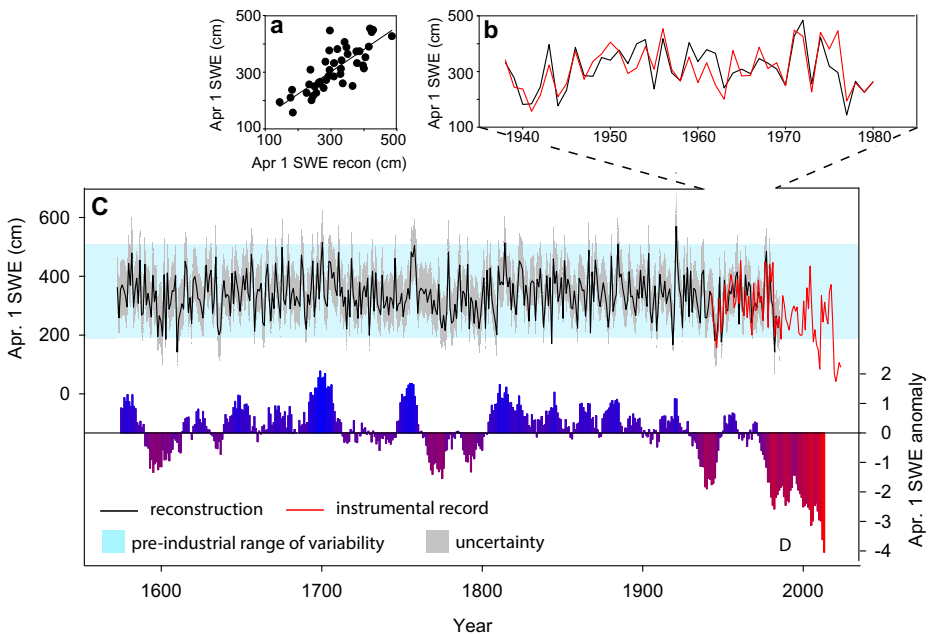

Fig. 3 North Cascades April 1 SWE reconstruction. (A) Scatter plot of instrumental April 1 SWE values and reconstructed values 1938–1980. (B) Reconstruction model plotted as instrumental (red) and reconstructed (black) April 1 SWE values for the North Cascades reconstruction during the period 1938–1980 ($R^2 = 0.61$, $p < 0.0001$). (C) Reconstructed April 1 SWE 1580–1980 (black) with instrumental data (red) plotted 1938–2018 for the North Cascades. Time series shown are annual reconstruction values (black) with the uncertainty envelope (5% and 95%; gray). Pre-industrial range of variability estimated as the 99th (508.4) and 1st (188.8) percentiles of the data prior to 1900. (D) 11-year standardized anomalies for the North Cascades April 1 SWE reconstruction

forward nests corroborated that trees followed the most recent snowpack trends while high-lighting the need to update these key chronologies through the most recent decades to better reduce uncertainties.

3.3 Reconstructed North Cascades April 1 SWE

We provide a 400-year (1580-1980 CE) annual reconstruction of April 1 SWE that accounts for 62% of the instrumental period variability (1938–1980) (Fig. 3). Snowpack during 2015 was also the lowest captured during the instrumental period 1938–2018 (Fig. S3). In agreement with the instrumental data, the reconstruction indicates that the 2014–2018 snow drought was unprecedented in magnitude, with 2015 witnessing the lowest snowpack since the beginning of the record (Figs. S3, 3). The 2015 SWE value also exceeds the 5% (low) MEBoot model uncertainty error envelope calculated over this 400-year period.

The 2014–2016 northern Cascades snow drought—especially snow conditions during the 2015 winter—is unprecedented within the context of the last 400 years. This trend is also consistent with anomalously low snowpack in the Sierra Nevada Mountains (e.g., Belmecheri et al. 2016), and thus part of a broader trend toward reduced snowpack in western North America. A blue intensity-derived growing season (May–Aug) temperature reconstruction from the Yukon Territory by Wilson et al. (2019) offers a regional comparison to our record. The spring-summer Yukon temperature record showed strong anti-
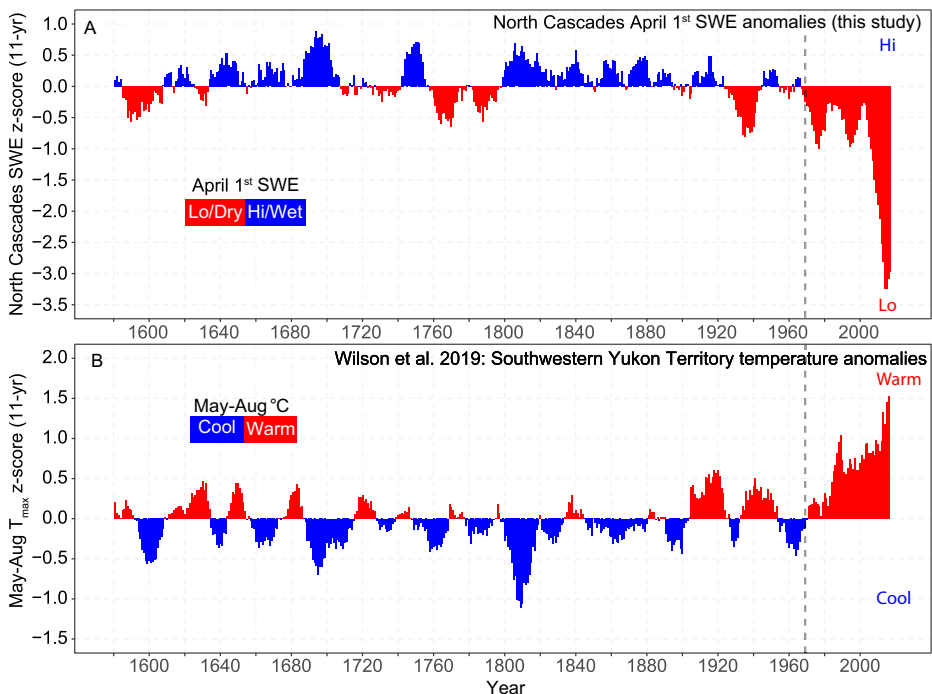

Fig. 4 Temperature influence on North Cascades April 1st SWE variability. (A) 11-year standardized anomalies for the North Cascades April 1 SWE reconstruction plotted with 11-year anomalies of May–Aug maximum temperature anomalies across southwestern Yukon Territory, Canada from Wilson et al. (2019)

correlation during the period 1580–2004 with snowpack anomalies from the North Cascades (Fig. 4; $r = -0.56$, $p < 0.00001$). The most noticeable correspondence between the records was the rapid warming across the region beginning in ca. 1900 simultaneous with the rapid decline in snowpack, especially since 1970 (dashed line Fig. 4). Within the context of single-year extremes, 1944 and 1915 ranked as the 3rd and 4th warmest since 1337 CE. The years 1914 and 1944 ranked as the 8th and 10th lowest snowpack years. The year 1810 ranked as the 2nd coldest year with the 3rd highest snowpack. Extreme SWE years occurred in 1697 (515.5 cm) and 1754 (505.4 cm), which were the 2nd and 5th highest on record (Table 3). The top 5 highest SWE decades (average cm) were the 1750s (391.2), 1700s (387.2), 1690s (377.2), 1840s (374.5), and 1810s (373.3), respectively. In conjunction with the Wilson et al. (2019) record, Wilson et al. (2014) built on the Wilson and Luckman (2003) and Luckman and Wilson (2005) studies and provide another proximal temperature record from interior, southern British Columbia. This record showed the lowest temperature anomalies over the last ca. 400 years (past 1000 years according to Luckman and Wilson 2005) centered on 1700, during which we demonstrated one of the highest SWE events in the North Cascades. Conversely, their temperature record showed above-average temperature anomalies

Table 3 Top 10 single-year and decadal low and high April 1 SWE (cm) events in the North Cascades reconstruction during the period 1580–2018

	Year	SWE	Decade	SWE
Low				
1	2015	42.7	2010	182.0
2	2016	71.6	1940	272.4
3	2014	79.3	1980	279.5
4	2018	91.7	1770	280.4
5	2017	106.4	2000	284.2
6	1607	142.5	1590	294.7
7	1977	144.0	1990	296.8
8	1914	167.4	1600	296.9
9	1839	171.1	1790	301.1
10	1944	177.0	1970	309.1
High				
1	1916	569.3	1750	391.2
2	1697	515.5	1700	387.2
3	1810	513.3	1690	377.2
4	1880	509.7	1840	374.5
5	1754	505.4	1810	373.3
6	1991	503.8	1880	365.9
7	1672	498.1	1570	362.5
8	1862	488.1	1650	358.7
S 9	1972	484.8	1860	351.8
10	1775	482.4	1890	351.5

Decade, e.g., 1940, defined as 1940–1949, except 2010–2018

starting in the 1930s and continuing through the 1950s to the current period, concurrent with below-average SWE anomalies and the recent snow drought.

Major periods of synchronous cool/high snowpack conditions included the 1690s–1710s, 1800s–1820s, 1840s–1880s. However, after the 1880s, there was a marked shift to synchronous periods of warm/low snowpack conditions. Because snowpack is a critical component to the water resources of the western US, many studies have observed trends in both temperature and precipitation during the twentieth century (e.g., McCabe and Wolock 2002; Mote 2003; Sheppard et al. 2002; Mote et al. 2016; Harpold and Brooks 2018) as well as the influence of temperature on earlier spring snowmelt during this period of rapid warming (e.g., Dettinger and Cayan 1995; Stewart et al. 2005; Regonda et al. 2005; Cooper et al. 2016; Sproles et al. 2017). Mote et al. (2005) concluded that some of the long-term trends in snowpack decline and short-term variability can be linked to Pacific climate forcing via
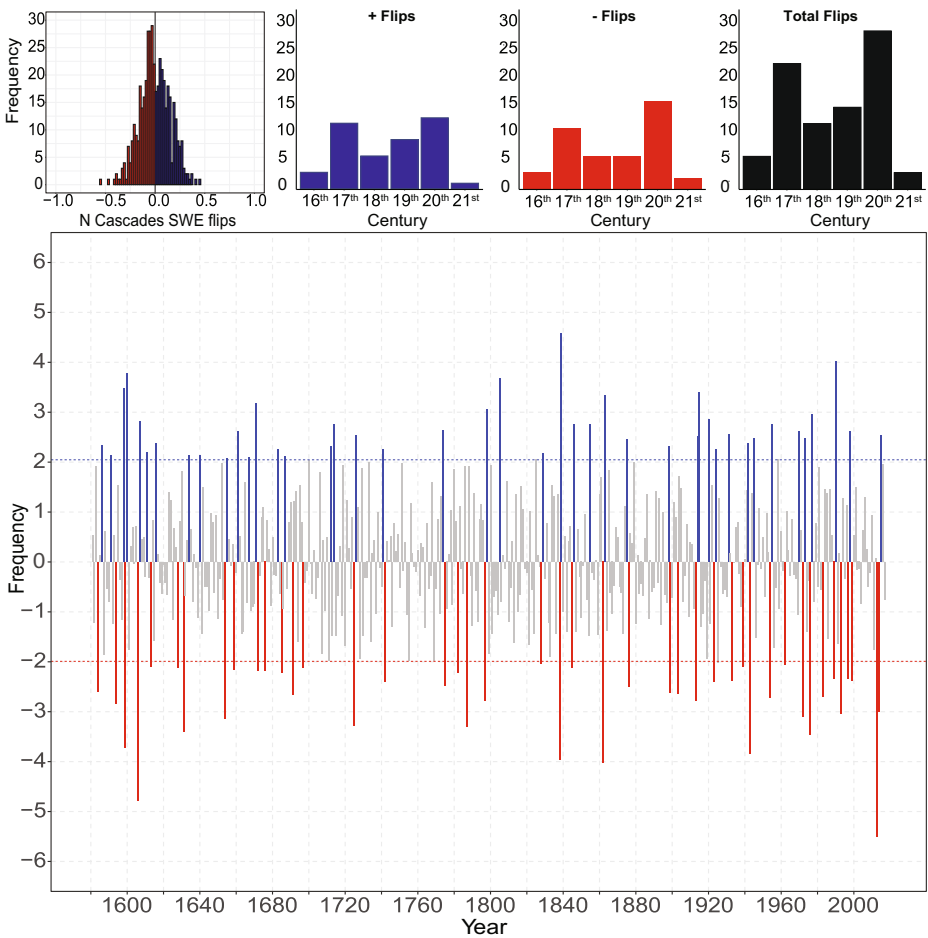
Fig. 5 North Cascades April 1 SWE volatility. Plotted are the annual flip index time series (bottom), shown with the frequency distribution for the annual flip index (top left), and the number of positive (+), negative (−), and total flips that exceed the 5th and 95th percentiles per century. The bottom panel shows the annual flip index with positive (blue) and negative (red) 5th and 95th percentile lines

El Nino-Southern Oscillation and Pacific Decadal Variability. Yet, climate variability over the North Pacific Ocean only accounted for ca. 50% of the declining snowpack trends since ca. 1950, whereas the remaining trend was explained by warming air temperatures across the Pacific Northwest US. Mote et al. (2016) reached a similar conclusion for the causes of the 2014–2015 snow drought across the North Cascades. They found that unusually high air temperatures converged with anomalously warm sea surface temperatures in the Northeast Pacific directly off the US Pacific Northwest coast (i.e., Bond et al. 2015; coined the "blob" by the media) to result in a warm winter and extremely low snowfall. We also found a strong anti-correlations between Cascades snowpack and Dec–Feb Northeast Pacific SSTs ($r < -0.60$, $p < 0.10$) during the period 1870–1999 (Fig. S4). Yet the April 1 SWE record from the North Cascades in comparison with the Yukon Territory temperature record suggests the influence of increased air temperature on anomalously low snowpack conditions is unique to the twentieth-twenty-first centuries and unprecedented within the context of the past 400 years.

Not only is the twentieth–twenty-firstcentury period characterized by the rapid decline in snowpack conditions, it is also highly volatile (Fig. 5). The northern Cascades flip index shows that, at least for the past 400 years, year-to-year changes in extreme snowpack conditions did occur, but with varying intensity over time. Since 1580, negative flips (year-to-year change from wet to dry) were more frequent than positive flips. When only considering flip
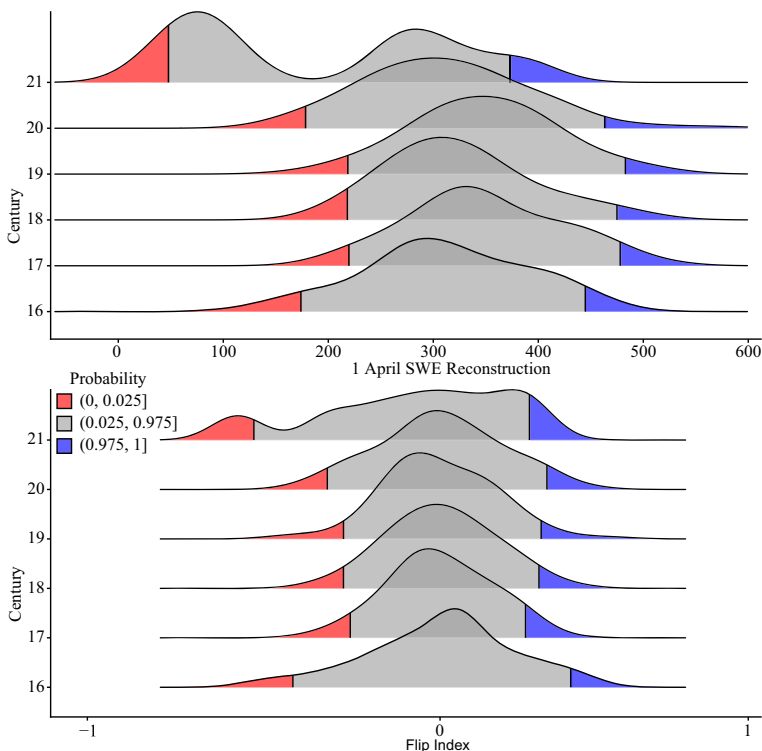

Fig. 6 Ridgeplots of North Cascades April 1 SWE Reconstruction and Flip Index Distributions by Century. Plotted are reconstruction and flip index values by century (sixteeth-twenty-first) with 2.5% (red) and 97.5% (blue) tails indicated

index values that exceeded the 5th and 95th percentiles, negative flips outnumber positive flips as tallied per century except for the seventeenth century, but this is likely explained by the influence of the Maunder Minimum (Lean 2000). More positive and negative flips (<5th >95th percentiles) occurred during the twentieth century ($n = 29$) than any century since the beginning of the record. Probability density functions calculated for the reconstruction and the flip index for each century also demonstrate that extreme flips during the twentieth and twenty-first centuries were anomalous within the context of the past ca. 430 years (Fig. 6). This finding is in line with multiple other studies that have shown that one of the characteristics of recent climate change is increased volatility in weather across the Pacific (Black et al. 2014; Black et al. 2018; Mantua 2015), American Southwest hydroclimate (Oliver et al. 2019), California precipitation (Swain et al. 2018), and western US wildfire activity (Abatzoglou and Williams 2016; Balch et al. 2017; Westerling et al. 2006).

Beyond the recent snow drought, the reconstruction identified other low snowpack events during the periods 1585–1605, 1760–1795, and 1920–1940, all of which are concurrent with anomalously warm decades identified by Wilson et al. (2019). Yet, these events were not as severe nor prolonged as that during the most recent decades. Six of the top 10 lowest SWE decades occurred during the twentieth-twenty-first centuries (1940, 1970, 1980, 1990, 2000, 2010; Table 3). The last 8 years of analysis, defined here as the 2010 decade (2010–2018), was by far the decade with the lowest average snowpack (182.0 cm), followed by the 1940s (272.4 cm). Rounding out the top 5 most extreme single-year (cm) low SWE conditions were 2015 (42.7 cm), 2016 (71.6), 2014 (79.3), 2018 (91.7), and 2017 (106.4), respectively. Furthermore, we note a large difference between the top 5 low SWE years and those ranked 6th–10th, with 1607 at 142.5 cm.

During the period 1932–1938, the Dust Bowl was characterized by widespread, severe drought conditions in the Great Plains and western North America (e.g., Cook et al. 2008). Schubert et al. (2004) produced model results suggesting the 1930s' Dust Bowl was caused by anomalously cool tropical sea surface temperatures in the Pacific Ocean. While this caused reduced precipitation over the Great Plains, it also produced wet anomalies in the Pacific Northwest region. SST anomalies in the Gulf of Alaska were above average during the Dust Bowl (Schubert et al. 2004) but do not compare to the extremely positive (warm) SST anomalies in the northern Pacific that led to the most recent snow drought (Bond et al. 2015). Hence, we noted average SWE conditions during the 1932–1938 period, which was concurrent with a period of cool air temperatures (Fig. 4). Following the Dust Bowl event, however, SWE conditions continued to decline heading into the 1940s, concurrent with warmer than average air temperatures. Thus, our record suggests the imprint of the Dust Bowl was minimal on northern Cascades winter precipitation, as Schubert et al. (2004) ultimately conclude that summer and fall seasonal SST anomalies in the tropical Pacific are likely key to better understanding the mechanisms of the event. Moreover, another severe western drought occurred in the 1950s (Cook et al. 1999), but evidence of associated low snowpack was not apparent in the instrumental record nor the tree-ring-based SWE reconstruction (Fig. 3). The 1950s was the last period during which snowpack anomalies were positive, after which began the rapid and unprecedented decline through to the present.

Pederson et al. (2011) documented the recent decline in western US snowpack and provided separate reconstructions for the Northern Rockies, Greater Yellowstone, and Upper Colorado Basin regions. It should be noted that only two tree-ring chronologies—Hart's Pass N2 (WA073) and V2 (WA077)—are used in both the Northern Rockies SWE reconstruction (total n=28, Pederson et al. 2011) and the record provided here; hence, the two reconstructions are not fully independent. The Northern Rockies (HUC 6) April 1 SWE reconstruction from Pederson et al. (2011) shows significant and positive agreement

with the northern Cascades record during the period of overlap (1580–1990; $r = 0.30$, p <0.0001; Fig. S5a). Other than a few outliers, most values fall within the 95% prediction bands (Fig. S5b). Despite diverging during the nineteenth century, the two records strongly correspond from the late 1500s through the 1700s, then again starting at ca. 1900 to the 1990s. Since the 1580s, snowpack conditions between the Northern Rockies and the North Cascade regions were in general synchrony. Yet, within the context of broader spatial heterogeneity across the western US, low snowpack conditions during the late sixteenth century were concurrent with drought across the Upper Colorado Basin (Woodhouse 2003; Pederson et al. 2011). However, snowpack conditions during this time were average in the Northern Rockies/Upper Columbia River Basin and Greater Yellowstone Regions. Pederson et al. (2011) also note two event periods during which snowpack conditions were higher than average across the northern American Cordillera ca. 1695–1735 and 1845–1895, and these also are noted across the northern Cascades.

4 Conclusions

Across the North Cascades of Washington, snowpack in 2015 (42.7 cm) was the lowest in at least the past 400 years, even when considering the 5% confidence interval estimates. Not only was mean winter air temperature across the Cascades highest on record during the middle 2010s, this event co-occurred with the appearance of extremely warm (positive) SST anomalies manifested directly off the coast of the Pacific Northwest (Fig. S4), strengthened by the stagnation of high pressure in the Gulf of Alaska (Bond et al. 2015). This extremely strong ridge of high pressure increased temperatures in the region and led to record-level snowpack reductions.

The increased volatility of Pacific climate forcing suggests that snowpack conditions will likely not stabilize. Since 1580, more extreme snowpack flips have occurred since 1900 than in any previous century. Increased snowpack volatility has important implications for current and future regional water allocation planning. The unprecedented decline in snowpack will fundamentally impact regional drought and hydrography in North Cascadia and is likely the combined result of rising temperatures, weakening westerly winds, and the magnitude and timing of winter precipitation events.

References

Abatzoglou JT, Williams AP (2016) Impact of anthropogenic climate change on wildfire across western us forests. Proc Natl Acad Sci 113(42):11770–11775

Akaike H (1974) A new look at the statistical model identification. In: Selected papers of Hirotugu Akaike. Springer, pp 215–222

Balch JK, Bradley BA, Abatzoglou JT, Nagy RC, Fusco EJ, Mahood AL (2017) Human-started wildfires expand the fire niche across the united states. Proc Natl Acad Sci 114(11):2946–2951

Bales RC, Molotch NP, Painter TH, Dettinger MD, Rice R, Dozier J (2006) Mountain hydrology of the western united states. Water Resour Res 42:8

Barnett T, Adam Y, Lattermaier C (2008) Potential impact of a warm climate on water availability in a snow dominated region

Bekker MF, Justin DeRose R, Buckley BM, Kjelgren RK, Gill NS (2014) A 576-year weber river streamflow reconstruction from tree rings for water resource risk assessment in the wasatch front, Utah. JAWRA J Am Water Resour Assoc 50(5):1338–1348

Belmecheri S, Babst F, Wahl ER, Stahle DW, Trouet V (2016) Multi-century evaluation of Sierra Nevada snowpack. Nat Clim Change 6(1):2

Black BA, Sydeman WJ, Frank DC, Griffin D, Stahle DW, García-Reyes M, Rykaczewski RR, Bograd SJ, Peterson WT (2014) Six centuries of variability and extremes in a coupled marine-terrestrial ecosystem. Science 345(6203):1498–1502

Black BA, van der Sleen P, Di Lorenzo E, Griffin D, Sydeman WJ, Dunham JB, Rykaczewski RR, García-Reyes M, Safeeq M, Arismendi I et al (2018) Rising synchrony controls western north american ecosystems. Global Change Biol 24(6):2305–2314

Bond NA, Cronin MF, Freeland H, Mantua N (2015) Causes and impacts of the 2014 warm anomaly in the ne pacific. Geophys Res Lett 42(9):3414–3420

Cook ER, Peters K (1981) The smoothing spline: a new approach to standardizing forest interior tree-ring width series for dendroclimatic studies

Cook ER, Meko DM, Stahle DW, Cleaveland MK (1999) Drought reconstructions for the continental united states. J Climate 12(4):1145–1162

Cook ER, Woodhouse CA, Eakin CM, Meko DM, Stahle DW (2004) Long-term aridity changes in the western united states. Science 306(5698):1015–1018

Cook ER, Seager R, Cane MA, Stahle DW (2007) North American drought: reconstructions, causes, and consequences. Earth-Sci Rev 81(1-2):93–134

Cook BI, Miller RL, Seager R (2008) Dust and sea surface temperature forcing of the 1930s "dust bowl" drought. Geophys Res Lett 35:8

Cook ER, Palmer JG, Ahmed M, Woodhouse CA, Fenwick P, Zafar MU, Wahab M, Khan N (2013) Five centuries of upper indus river flow from tree rings. J Hydroly 486:365–375

Cooper MG, Nolin AW, Safeeq M (2016) Testing the recent snow drought as an analog for climate warming sensitivity of cascades snowpacks. Environ Res Lett 11(8):084009

Coulthard B, Smith DJ, Meko DM (2016) Is worst-case scenario streamflow drought underestimated in British Columbia? A multi-century perspective for the South Coast, derived from tree-rings. J Hydrol 534:205–218

Dettinger MD, Cayan DR (1995) Large-scale atmospheric forcing of recent trends toward early snowmelt runoff in california. J Climate 8(3):606–623

Flanner MG, Shell KM, Barlage M, Perovich DK, Tschudi M (2011) Radiative forcing and albedo feedback from the northern hemisphere cryosphere between 1979 and 2008. Nat Geosci 4(3):151

Fritts H (1976) Tree rings and climate. Elsevier

Graumlich LJ (1987) Precipitation variation in the pacific northwest (1675–1975) as reconstructed from tree rings. Ann Assoc Am Geogr 77(1):19–29

Graumlich LJ, Brubaker LB (1986) Reconstruction of annual temperature (1590–1979) for longmire, Washington, derived from tree rings. Quatern Res 25(2):223–234

Griffin D, Woodhouse CA, Meko DM, Stahle DW, Faulstich HL, Carrillo C, Touchan R, Castro CL, Leavitt SW (2013) North american monsoon precipitation reconstructed from tree-ring latewood. Geophys Res Lett 40(5):954–958

Guttman L (1954) Some necessary conditions for common-factor analysis. Psychometrika 19(2):149–161

Hansen-Bristow K (1986) Influence of increasing elevation on growth characteristics at timberline. Can J Bot 64(11):2517–2523

Harpold AA, Brooks PD (2018) Humidity determines snowpack ablation under a warming climate. Proc Natl Acad Sci 115(6):1215–1220

Harley GL, Maxwell JT (2018) Current declines of pecos river (New Mexico, USA) streamflow in a 700-year context. The Holocene 28(5):767–777

Harley GL, Maxwell JT, Larson E, Grissino-Mayer HD, Henderson J, Huffman J (2017) Suwannee river flow variability 1550–2005 ce reconstructed from a multispecies tree-ring network. J Hydrol 544:438–451

Hart SJ, Smith DJ, Clague JJ (2010) A multi-species dendroclimatic reconstruction of chilko river streamflow, British Columbia, Canada. Hydrol Process 24(19):2752–2761

Hauer FR, Baron JS, Campbell DH, Fausch KD, Hostetler SW, Leavesley GH, Leavitt PR, McKnight DM, Stanford JA (1997) Assessment of climate change and freshwater ecosystems of the rocky mountains, usa and canada. Hydrol Process 11(8):903–924

Holmes R (1983) Program cofecha user's manual laboratory of tree-ring research. The University of Arizona, Tucson

Kaiser HF (1960) The application of electronic computers to factor analysis. Educ Psychol Measur 20(1):141–151

Lean J (2000) Evolution of the sun's spectral irradiance since the maunder minimum. Geophys Res Lett 27(16):2425–2428

Littell JS, McKenzie D, Peterson DL, Westerling AL (2009) Climate and wildfire area burned in western us ecoprovinces, 1916–2003. Ecol Appl 19(4):1003–1021

Loecke TD, Burgin AJ, Riveros-Iregui DA, Ward AS, Thomas SA, Davis CA, Clair MAS (2017) Weather whiplash in agricultural regions drives deterioration of water quality. Biogeochemistry 133(1):7–15

Luckman B, Wilson R (2005) Summer temperatures in the canadian rockies during the last millennium: a revised record. Climate Dynam 24(2–3):131–144

Mantua NJ (2015) Shifting patterns in pacific climate, west coast salmon survival rates, and increased volatility in ecosystem services. Proc Natl Acad Sci 112(35):10823–10824

Margolis EQ, Meko DM, Touchan R (2011) A tree-ring reconstruction of streamflow in the santa fe river, new mexico. J Hydrol 397(1–2):118–127

Maxwell RS, Harley GL, Maxwell JT, Rayback SA, Pederson N, Cook ER, Barclay DJ, Li W, Rayburn JA (2017) An interbasin comparison of tree-ring reconstructed streamflow in the Eastern United States. Hydrol Process 31(13):2381–2394

McCabe GJ, Wolock DM (2002) Trends and temperature sensitivity of moisture conditions in the conterminous united states. Climate Res 20(1):19–29

Meko DM, Woodhouse CA, Baisan CA, Knight T, Lukas JJ, Hughes MK, Salzer MW (2007) Medieval drought in the upper Colorado river basin. Geophys Res Lett 34:10

Melvin T, Briffa K (2008) A 'signal-free' approach to dendroclimatic standardisation. Dendrochronologia 26(2):71–86

Mote PW (2003) Trends in snow water equivalent in the pacific northwest and their climatic causes. Geophys Res Lett 30:12

Mote PW, Hamlet AF, Clark MP, Lettenmaier DP (2005) Declining mountain snowpack in western north america. Bull Am Meteorol Soc 86(1):39–50

Mote PW, Rupp DE, Li S, Sharp DJ, Otto F, Uhe PF, Xiao M, Lettenmaier DP, Cullen H, Allen MR (2016) Perspectives on the causes of exceptionally low 2015 snowpack in the western United States. Geophys Res Lett 43(20):10–980

Oliver JS, Harley GL, Maxwell JT (2019) 2,500 years of hydroclimate variability in New Mexico, USA. Geophys Res Lett 46(8):4432–4440

Pederson GT, Graumlich LJ, Fagre DB, Kipfer T, Muhlfeld CC (2010) A century of climate and ecosystem change in western montana: what do temperature trends portend? Clim Change 98(1–2):133–154

Pederson GT, Gray ST, Woodhouse CA, Betancourt JL, Fagre DB, Littell JS, Watson E, Luckman BH, Graumlich LJ (2011) The unusual nature of recent snowpack declines in the North American Cordillera. Science 333(6040):332–335

Perkins DL, Swetnam TW (1996) A dendroecological assessment of whitebark pine in the sawtooth–salmon river region, Idaho. Can J Forest Res 26(12):2123–2133

Peterson DW, Peterson DL (1994) Effects of climate on radial growth of subalpine conifers in the north cascade mountains. Can J Forest Res 24(9):1921–1932

Regonda SK, Rajagopalan B, Clark M, Pitlick J (2005) Seasonal cycle shifts in hydroclimatology over the Western United States. J Clim 18(2):372–384

Salzer MW, Kipfmueller KF (2005) Reconstructed temperature and precipitation on a millennial timescale from tree-rings in the southern colorado plateau, USA. Clim Change 70(3):465–487

Schubert SD, Suarez MJ, Pegion PJ, Koster RD, Bacmeister JT (2004) On the cause of the 1930s dust bowl. Science 303(5665):1855–1859

Sheppard PR, Comrie AC, Packin GD, Angersbach K, Hughes MK (2002) The climate of the us southwest. Climate Res 21(3):219–238

Speer JH (2010) Fundamentals of tree-ring research. University of Arizona Press

Sproles EA, Roth TR, Nolin AW (2017) Future snow? A spatial-probabilistic assessment of the extraordinarily low snowpacks of 2014 and 2015 in the oregon cascades. Cryosphere 11(1):331

Stahle DW, Cleaveland MK, Grissino-Mayer HD, Griffin RD, Fye FK, Therrell MD, Burnette DJ, Meko DM, Villanueva Diaz J (2009) Cool-and warm-season precipitation reconstructions over Western New Mexico. J Climate 22(13):3729–3750

Starheim CC, Smith DJ, Prowse TD (2013) Dendrohydroclimate reconstructions of july–august runoff for two nival-regime rivers in West Central British Columbia. Hydrol Process 27(3):405–420

Stewart IT, Cayan DR, Dettinger MD (2005) Changes toward earlier streamflow timing across Western North America. J Clim 18(8):1136–1155

Stockton CW, Jacoby GC (1976) Long-term surface water supply and streamflow levels in the upper Colorado river basin. Lake powell research project. Bulletin 18:70

Stockton CW, Meko DM (1975) A long-term history of drought occurrence in western United States as inferred from tree rings. Weatherwise 28(6):244–249

Swain DL, Langenbrunner B, Neelin JD, Hall A (2018) Increasing precipitation volatility in twenty-first-century California. Nat Clim Change 8(5):427

Vinod HD, López-de Lacalle J et al (2009) Maximum entropy bootstrap for time series: the meboot r package. J Stat Softw 29(5):1–19

Watson E, Luckman BH (2016) An investigation of the snowpack signal in moisture-sensitive trees from the Southern Canadian Cordillera. Dendrochronologia 38:118–130

Westerling AL, Hidalgo HG, Cayan DR, Swetnam TW (2006) Warming and earlier spring increase western us forest wildfire activity. Science 313(5789):940–943

Wigley TML, Briffa KR, Jones PD (1984) On the average value of correlated time series, with applications in dendroclimatology and hydrometeorology. J Clim Appl Meteor 23:201–213

Wilson RJ, Luckman BH (2003) Dendroclimatic reconstruction of maximum summer temperatures from upper treeline sites in interior British Columbia, Canada. The Holocene 13(6):851–861

Wilson R, Rao R, Rydval M, Wood C, Larsson LÅ, Luckman BH (2014) Blue intensity for dendroclimatology: the bc blues: a case study from British Columbia, Canada. The Holocene 24(11):1428–1438

Wilson R, Anchukaitis K, Andreu-Hayles L, Cook E, D'Arrigo R, Davi N, Haberbauer L, Krusic P, Luckman B, Morimoto D et al (2019) Improved dendroclimatic calibration using blue intensity in the Southern Yukon. The Holocene p 0959683619862037

Woodhouse CA (2003) A 431-yr reconstruction of western Colorado snowpack from tree rings. J Climate 16(10):1551–1561

Woodhouse CA, Gray ST, Meko DM (2006) Updated streamflow reconstructions for the upper Colorado river basin. Water Resour Res 42:5

Woodhouse CA, Meko DM, MacDonald GM, Stahle DW, Cook ER (2010) A 1,200-year perspective of 21st century drought in Southwestern North America. Proc Natl Acad Sci 107(50):21283–21288

Woodhouse CA, Stahle DW, Díaz JV (2012) Rio grande and rio conchos water supply variability over the past 500 years. Climate Res 51(2):147–158

Affiliations

Grant L. Harley[1] · R. Stockton Maxwell[2] · Bryan A. Black[3] · Matthew F. Bekker[4]

[1] Idaho Tree-Ring Lab, Department of Geography, University of Idaho, Moscow, ID, 83843, USA

[2] Department of Geospatial Science, Radford University, Radford, VA 24142, USA

[3] Laboratory of Tree-Ring Research, University of Arizona, Tucson, AZ 85721, USA

[4] Department of Geography, Brigham Young University, 690 KMBL, Provo, UT 84602, USA